J Mater Sci (2006) 41:6830–6842
DOI 10.1007/s10853-006-0374-3

Role of skin/core structure and inclusions in the fatigue crack initiation and propagation in organic fibres

C. Le Clerc · A. R. Bunsell · A. Piant · B. Monasse

Received: 3 March 2006 / Accepted: 25 April 2006 / Published online: 27 September 2006

Abstract High performance polyamide and polyester thermoplastic fibres fail by a distinct fatigue process but the microstructural phenomena involved in crack initiation, have, until now, been difficult to interpret. The process of crack initiation has been revealed as being associated with the presence of small solid inclusions, observed in all the studied fibres. The position of the inclusions is seen to be important and this may be explained in terms of fibre macroscopic morphology linked to the manufacturing process. The presence of a skin/core structure is revealed. The mechanical experiments used throughout this study were performed on single fibres with, numerous analyses being carried out using SEM, optical microscopy and birefringence techniques.

Introduction

High performance thermoplastic fibres find wide use in technical applications such as the reinforcement of tyres, belting, in the field of geotextiles or in assemblies of numerous yarns in mooring ropes or climbing ropes. For each use, the mechanical loading can differ and thus the required performance for each fibre. In the field of offshore moorings or geotextiles, the long time creep behaviour of fibres is the main limiting phenomenon. For all dynamic structures such as tyres and belting, the response to cyclic stress is of primary importance. The understanding of the initiation processes in the fatigue damage of fibres is the main topic of this study.

The typical morphology of broken fibres after a tensile test shows two symmetrical complementary ends with a bevelled region corresponding to subcritical crack growth and plastic deformation ahead of the crack tip followed by a region, perpendicular to the fibre axis, due to rapid crack propagation [1–5]. The typical longitudinal size of the damaged zone is less than a diameter. In the case of fatigue fracture at room temperature, the morphologies of the two broken ends are very different with one broken end revealing a long tongue removed from the other end, which, in this paper will be called the ''complementary end''. A longitudinal crack is initiated near the surface, it propagates, at a slight angle to the fibre axis, penetrating into the fibre and reducing the load bearing section [1–5]. Finally, the increase in stress causes failure by creep or tensile processes. That particular fracture leads to a damaged zone with a typical length of 20–50 diameters. This remarkable morphology reflects the high anisotropy of these fibres. The scope of this paper is to study the origin of this difference of initiation and propagation between tensile and fatigue fracture.

The standard industrial process for the fabrication of high performance organic fibres includes polymerization, high-speed spinning to enhance mechanical

C. Le Clerc (✉) · A. R. Bunsell · A. Piant
Centre des Matériaux Pierre et Marie Fourt, Ecole des Mines de Paris, U.M.R. CNRS 7633, BP 87, Evry Cedex 91003, France
e-mail: christophe.leclerc@ensmp.fr

B. Monasse
Centre de Mise en Forme des Matériaux, Ecole des Mines de Paris, Rue Claude Daunesse, Sophia Antipolis Cedex F-06904, France

properties and stretching. The rate of solid-state polycondensation of poly(ethylene terephthalate) is increased using catalysts such as antimony trioxide for polyester [6], and higher molecular weight confers better failure properties. High speed spinning is complex to analyse and the control of the strain-induced crystallisation is a key to obtain high performance fibres. Significantly, the cooling of the core of the fibre lags that of the surface layers so that residual stresses could be induced and result in a variation of properties within the fibre. Other additives are also used in fibres to improve some of properties such as resistance to oxidation and flame retardancy in polyamide 6.6 fibres by the addition of bromine components [7]. All these active additives can be introduced directly or supported on carriers, such as fumed silica. There are few papers presenting the role played by solid inclusions in an anisotropic material during mechanical loading. This study points out the effect of such particles.

The mechanical experiments including tensile tests and fatigue tests at room temperature, throughout this study, were performed on single fibres extracted from three different drawn yarns: two polyester yarns and a polyamide 6.6 yarn. Numerous analyses were carried out on fibres using optical microscopy, sometimes under polarized light, scanning electron microscopy with energy dispersive spectrometry, pyrolysis and sectioning with a microtome. This study deals with the fatigue crack initiation and propagation, emphasising particularly, the role of inclusions in the polymer and the role of the macroscopic morphology of the fibre induced during the fabrication process and their influence in determining the nature of the damage produced.

Material and methods

Material

Three different types of fibre were used in this study extracted from technical yarns. There were two poly(ethylene terephthalate) fibres, PET_A and PET_B and a polyamide 6.6 fibre (PA66). Their different mechanical characteristics are given in Table 1. These semi-crystalline, industrial fibres had been produced using high speed spinning so that the degree of crystallinity was about 50% and the molecular orientation was very high. The fibre diameters were between 18 and 27 μm and tensile strengths between 1 and 1.1 GPa.

Table 1 Characterization of the three different fibres studied

	PET_A	PET_B	PA66
Diameter	18.5 μm	21.5 μm	27.5 μm
Initial modulus	15 GPa	13 GPa	5 GPa
Tensile strength	1 GPa	1.05 GPa	1.1 GPa
Elongation at break	13%	16%	26%
Number of fibres in a yarn	390	250	210

Mechanical tests

The mechanical tests on single fibres were carried out on a universal fibre-testing machine developed by Bunsell et al. [1]. This apparatus is described elsewhere [2] and allowed tensile, creep and cyclic load tests to be performed on single fibres. The test could be load controlled or displacement controlled with very high accuracy. The load was monitored by a piezoelectric transducer with a sensitivity of 0.01 g ($9.81*10^{-5}$ N), the displacement of the cross-head by a LVDT transducer with a sensitivity of 1 μm and a capacitive transducer with a sensitivity of 6 μm monitoring the cyclic deformation produced by a vibrator acting on the same principal as a loud speaker. The fibre was held between two clamps, one mounted on the cross-head and connected by a screw thread to a motor controlled by a servosystem controlled by the chosen load or displacement. The other grip was fixed for tensile tests or connected to the vibrator for fatigue tests.

A tensile test consisted of a controlled increase of deformation at constant chosen speed until failure. For fatigue tests, a cyclic load, induced by the imposed cyclic deformation, was superimposed on a steady load and the maximum load maintained constant with automatic compensation for elongation due to creep or plastic deformation. The measured maximum load was continuously compared, by the servomechanism, to the required load level which was maintained constant to within 0.1 g ($9.81*10^{-4}$ N).

The apparatus could be used from 0 up to 100 g ($9.81*10^{-1}$ N), with a precision of 0.01 g ($9.81*10^{-5}$ N), a maximum displacement of 20 mm with a precision of 1 μm and a cyclic displacement, at 50 Hz, of up to ±3 mm. The gauge length used in this study was 30 mm. A cylindrical heater enabled experiments from 20 °C to 300 °C to be carried out. Tests in this study were conducted in the temperature range of 20–80 °C. The testing apparatus is shown in Fig. 1.

Scanning electron microscopy (SEM) observations

The scanning electron microscope used to observe fibre fracture morphologies is a field effect gun Zeiss Gemini DSM 982. The polymer samples were coated with a 3 nm layer of Gold/Palladium to avoid charging.

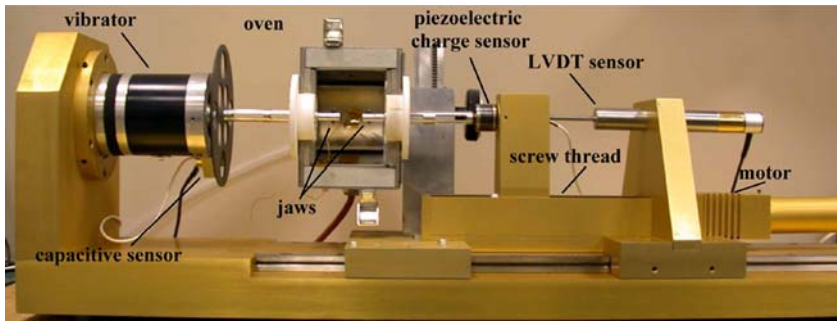

Fig. 1 Testing machine for single fibres, initially developed by Bunsell [5], with new modifications: oven and capacitive transducer

Observations were performed under two different conditions. For observations, the working distance was 3–4 mm to enhance resolution up to a magnification of 25,000, using a low electron beam accelerating voltage of 2 kV to minimize fibre damage. X-ray analyses however were carried out at a working distance of 10 mm for Energy Dispersive Spectrometry (EDS) using an accelerating voltage of 10 kV. This value gave a balance between excitation of energetic electrons whilst minimising of fibre damage or charge displacement under the beam.

Three kinds of EDS analyses were performed: spot, area spectrum and X-ray mapping of selected elements. In the latter case, point dwell map mode was selected with conditions chosen so as to minimize damage and displacement and to optimize count rate. The compromise meant low resolution but a medium exposure time for measurements, for example: a dwell time of 0.7 s for an X-ray map resolution of 32*32 pixels. The samples were precisely oriented in the beam using X/Y displacement, rotation and tilt to achieve maximum intensity and to avoid absorption.

Transmission optical microscopy

The main interest of transmission optical microscopy comes from the transparency of thick samples of polymers such as polyester or polyamide. Two microscopes were used in this study: a Reichert and a Leica equipped with a Nikon digital camera used with the Leica im1000 software. Several objectives with magnifications, from 20 to 100×, were used.

Fibres were held in between a slide and a cover glass and immersed in a mineral oil with a refractive index of 1.515, close to that of the polymer refractive index, in order to avoid optical reflection and refraction at the curved surface of the fibre. In the best optical conditions, the optical resolution was better than 0.4 μm. Polarized light was used to enhance contrast, especially using extinction conditions. As thermoplastic fibres are highly oriented, they present a high birefringence; the polarized light could in that case emphasize any local variation of birefringence of the material corresponding to a variation in orientation.

Yarn pyrolysis

To obtain data on the different elements added in the polymer fibres, pyrolysis of the yarns was performed for 1 h at 500 °C. This temperature assured the complete oxidation of the polymer and left most of the inclusions, such as fumed silica unchanged. The remaining fragments were spread on a carbon tape, metallised with 3 nm of Gold/Palladium and observed with the SEM. The nature and the typical size of the different inclusions could be determined by EDS analysis.

Microtomy

Microtome sectioning was carried out on fibres with an Ultracut Microtome from Leica. Fibres were embedded in a resin between two polyester films. Microtoming was performed at room temperature with a 35° diamond knife perpendicularly to the fibre axis and with a section thickness between 1 and 1.5 μm. These sections were collected from pure water using the capillarity induced with a whisker and then observed under the microscope.

Results

Visualization and characterisation of particles inside as-received fibres

The as-received fibres shown in Fig. 2 were photographed using polarized light. The birefringence of these fibres was found to be extremely high as the number of colour bands was high; previous measurements using a tilting B compensator gave a birefringence value of 0.212 for PET_A. One or two inclusions were observable for both the PET_A and PA66 fibres in the optical field of about 6 diameters, whereas more

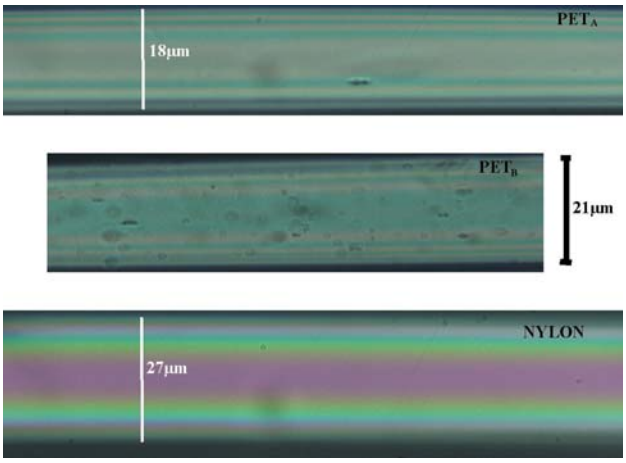

Fig. 2 Optical microscopy of as-received fibres under polarized light

than 50 were visible in the PET_B fibre, although most of them are out of focus in Fig. 2. Indeed, polymer fibres could be seen as a kind of composite with incorporated particles of different concentrations, compositions, sizes, moduli, dispersed within the polymer depending on each industrial process.

In order to identify the various inclusions in the different polymers, specimens of the PA66 and PET_B fibres were pyrolised under conditions in which most of the polymer molecules were volatilized. This then allowed EDS analyses to be conducted. The results concerning polyamide 6.6 are presented in Fig. 3. The elements found were oxygen, copper, zinc, bromine, silicon, phosphorus, potassium and traces of calcium. X-ray mapping allowed the following elements to be associated [K and P], [Cu, Zn, O], [Si with localised Br]. The characteristic length of the agglomerates was 0.7–1 μm. The results concerning PET_B are presented in Fig. 4. The elements found were oxygen, bromine, potassium, antimony, titanium and sodium. X-ray mapping allowed [K, P, Na, Sb], [Ti, O] to be associated. The characteristic length of the agglomerate was 0.4–0.7 μm.

Random blind EDS analyses were performed on PET_B fibres as they showed many inclusions; an oblique section of the fibre was made so as to maximize the section size. In two cases (one is shown on Fig. 5), a particle containing titanium was found in the polymeric matrix, its size was about 0.6 μm.

Mechanical tests on single fibres

Tensile tests

Tensile tests were performed on the three different types of fibres at a strain rate of 1%/s so as to obtain median breaking loads for various isothermal conditions. The results were around 1.00 GPa ± 0.018 GPa for PET_A, 1.10 GPa ± 0.066 GPa for PET_B and 1.05 GPa ± 0.03 GPa at room temperature. These values were used to fix the conditions used for fatigue tests as the tests were carried out at different levels of simple tensile breaking load (75%, 80%).

The fracture morphologies of fibres broken in tension and observed by SEM are shown in Fig. 6a and b. A two-phase propagation process can be seen, as described above, with a region of low speed crack propagation, associated with a plastic deformation ahead of the crack tip and then a rapid crack propagation perpendicular to the axis. There was no morphological difference between the fracture surfaces of the PET and PA66 fibres.

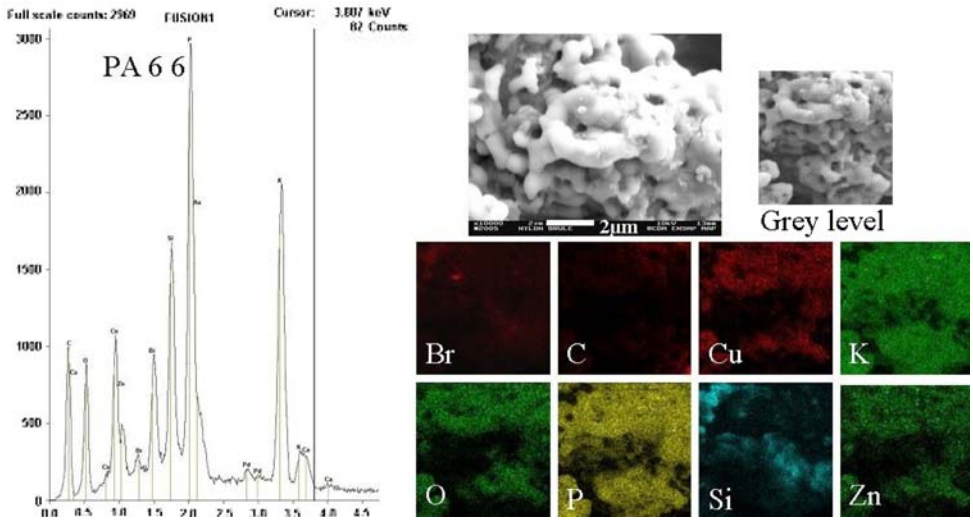

Fig. 3 EDS analysis of pyrolysed residues of Nylon yarn. Large area spectrum live acquisition time 200 s and X-ray map (point dwell map parameters: 128*128, 0.2 s)

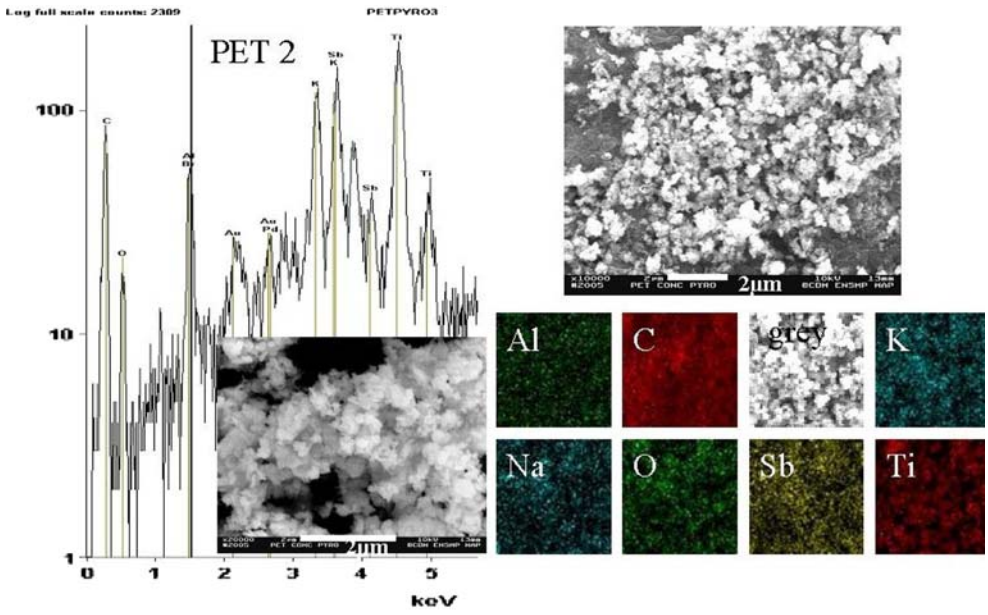

Fig. 4 EDS analysis of pyrolysed residus of PET_B yarn. Large area spectrum live acquisition time 200 s and X-ray map (point dwell map parameters: 64*64, 0.2 s)

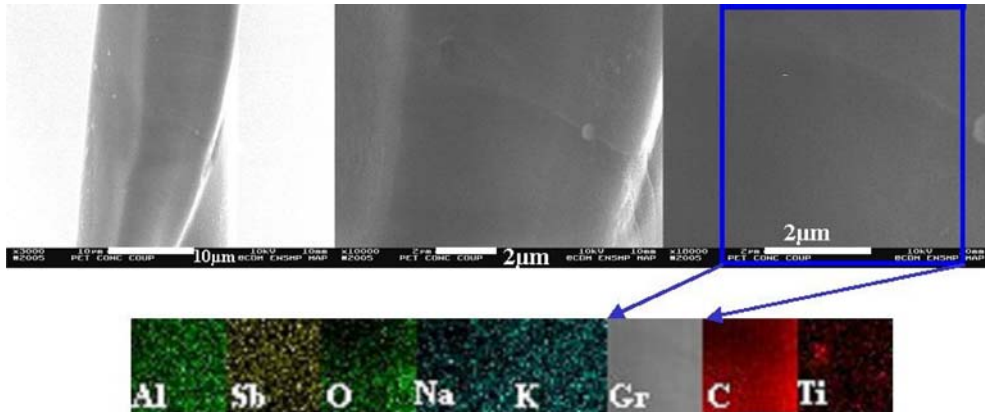

Fig. 5 SEM observations of an obliquely sectioned PET_B fibre, revealing particles containing Ti determined by X-ray mapping (point dwell map parameters: 32*32, 0.7 s)

Fatigue tests

Fatigue tests were carried out for various mechanical conditions with a zero minimum load and a maximum load at 75% or at 80% of the tensile breaking load. The experiments were performed at 50 Hz for two different temperatures: 20 °C and 80 °C. The fracture morphologies of failed PET fibres shown in Fig. 6c and d correspond to a room temperature fatigue test, whereas e and f were obtained with fatigue tests at 80 °C. The fracture morphologies obtained with the PET_A fibres at 20 °C are classical examples of the type, one broken end shows a tongue of material and the other is complementary. These fatigue fractures at room temperature are very different from tensile fractures obtained at the same temperature shown on Fig. 6a and b. These fatigue fractures, obtained at room temperature have been observed in many studies [1–4]. In contrast, at 80 °C, two symmetrical ends, each with a truncated tongue on both faces, were observed and this has been reported elsewhere [5]. At room temperature, morphological differences have been revealed in the fatigue failures of PET and PA66 fibres. The angle of crack penetration in fatigue was greater for PA66 than for PET, so that the final failure for this latter fibre appeared behind the fatigue crack tip and was due to the creep failure of the load supporting section. Final failure occurred at the tip of the fatigue crack in PA66 fibres and the load bearing section finally failed in tension.

In some cases, fatigue tests were stopped after the longitudinal crack began to propagate but before final failure. In order to do this in a reasonably controlled manner the cyclic strain amplitude was increased, during a maximum load controlled fatigue test, so that the fibres could be seen, with the aid of a stroboscope,

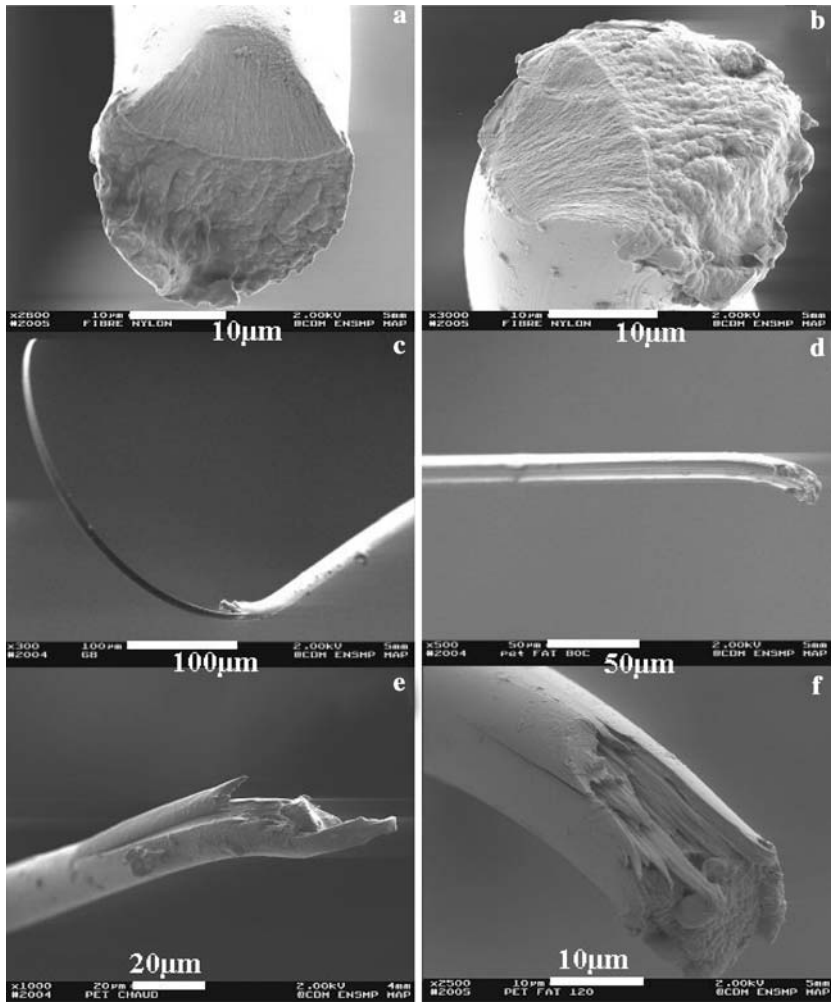

Fig. 6 Typical fracture morphologies observed with SEM obtained with PA66 fibres after a tensile test (**a**, **b**), on PET fibres after fatigue test at room temperature (**c**, **d**) and on PET_A fibres after a fatigue test at 80 °C (**e**, **f**)

to slightly buckle. Initially the fibre could be seen to buckle with a harmonic waveform however as soon as the fatigue crack began to propagate the fibre buckled as though it were creased at the point of fracture. The test could then be stopped and the cracked fibre examined. An example is given in Fig. 7. It can be seen that the tip of what would become the tongue has retracted away from the point of crack initiation, indicating either the relaxation of residual stresses in the tongue or the creep strain of the remaining load bearing section. The upper fractograph in Fig. 7 shows that, after initiation, the fracture began to propagate in both directions along the fibre.

Observation of inclusions near fatigue crack initiation points

Examples of PET fibres failed by the fatigue process, at room temperature, and observed by optical microscopy are presented in Fig. 8. Images a and b were taken

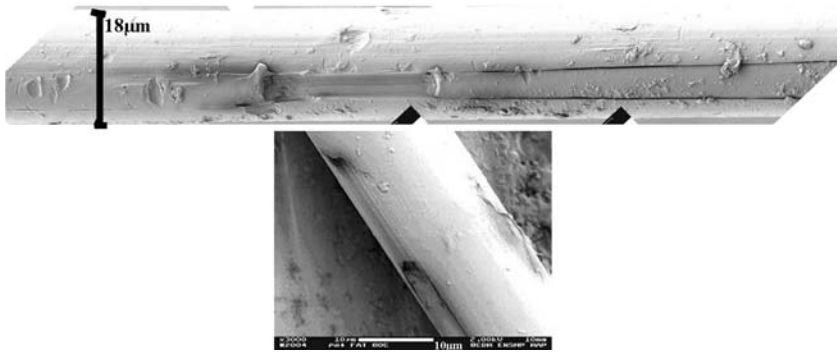

Fig. 7 Interrupted fatigue test on PET_A after cycling, observed by SEM

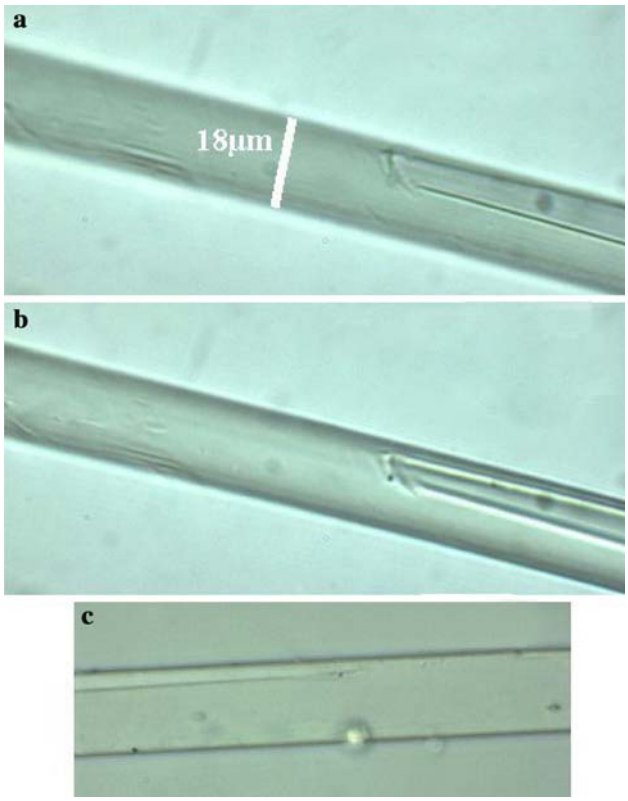

Fig. 8 Optical microscopy observations of the complementary end of PET fibre failed by fatigue, different depths of focus for **a** and **b**

from the same complementary part of failed fibre with the focus changed: the focal point was on the sides of the crack in image a and just inside the fibre in image b. In the latter picture, a black point can be seen just near the crack initiation point. In image c, an inclusion is visible just at the point of initiation of the crack.

Figure 9 shows an optical micrograph with natural light, looking down on the complementary fatigue fracture surface of a PET fibre. The main fatigue tongue has been removed from the upper left side of the image. A remaining part of that tongue can be seen on the upper side of the image. It is around 15 μm long and 1.5 μm thick. Near to one extremity of that tongue, there is an inclusion visible, around 2 μm from the fibre surface. An observation of the zone near the inclusion, with polarized light, underlines the perturbations induced by the inclusion in the surrounding polymer. In this and other similar cases, the particle sizes were found to be around 1 μm or less, similar to the characteristic size of the inclusions observed after pyrolysis. Many other similar observations have been made in the course of this study so that the association of crack initiation with inclusions seems to be established.

It was not possible to identify, by optical microscopy, the nature of the inclusions observed to be associated with crack initiation in the fibres. However SEM observations in the region of crack initiation, together with EDS X-ray mapping of fibres failed in fatigue, allowed some inclusions to be observed and identified. Figure 10 shows an initiation point, observed after a fatigue test, which led to failure at another point. A particle is visible on the surface of the fibre, the nature of which was revealed by X-ray mapping as being calcium dust with a precise shape. But the silicon X-ray map gave two points at two

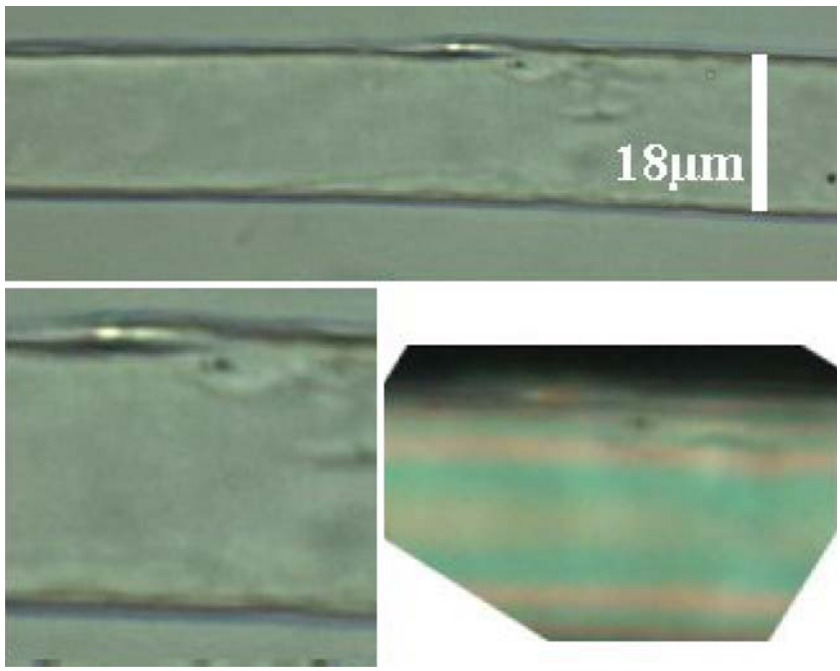

Fig. 9 Optical microscopy observations with natural light of complementary end of PET fibre failed by fatigue. The tongue is removed from the top left side of the fibre. The final image **c** was taken with polarized light

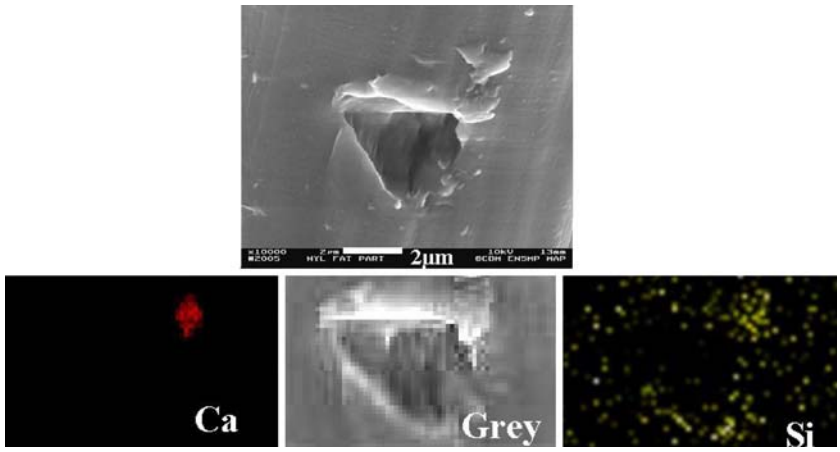

Fig. 10 SEM observation of fatigue crack initiation in PA66 fibres, with corresponding EDS X-ray map of Ca and Si

corners of the bevelled crack. This signal corresponds to inclusions, seen as hazy shapes, just under fibre surface.

Figure 11 shows the fracture morphology of a nylon fibre tested under conditions which induced fatigue at 80 °C; the observed morphology included a short longitudinal crack at the top right part and a subcritical tensile crack on the top left part of the failure. An EDS analysis revealed, just under the longitudinal crack, the presence of an inclusion in the otherwise carbon and oxygen background signal coming from the polymer. The signal associated silicon, bromine and oxygen compounds revealing that it must have been bromine, used as an antioxidant and fire retardant and carried on fumed silica.

Microtome sectioning of complementary ends of failed fibres

The complementary end of a PA66 fibre failed in fatigue was sectioned with the microtome to give sections of 1.5 µm thickness along 150 µm of the fibre. Of all the sections observed, eight are presented, in Fig. 12, in the direction of propagation. In the image a, the fibre surface is continuous but can be seen to be separated from the body of the fibre at the 12 o'clock position. A clear line is visible around the fibre circumference indicating the presence of a skin. In the image b, a crack is visible at the top whereas a second region of separation of the skin from the fibre body is visible at the bottom right part of the section. Images c–f, reveal that, the crack at the top of the section penetrates inside the fibre, so reducing the section; at the bottom part, the separated regions remain visible in all four images. The crack at the top of the images shows an irregular fatigue crack cross-section in contrast to image g in which the crack is more regular; however two new cracks can be seen to have been initiated at each side of the lower detached region. Image h is of a section close to the point of final failure. It can be seen in this latter image that the two cracks at the bottom have coalesced and the remaining section is less than 80% of the initial section.

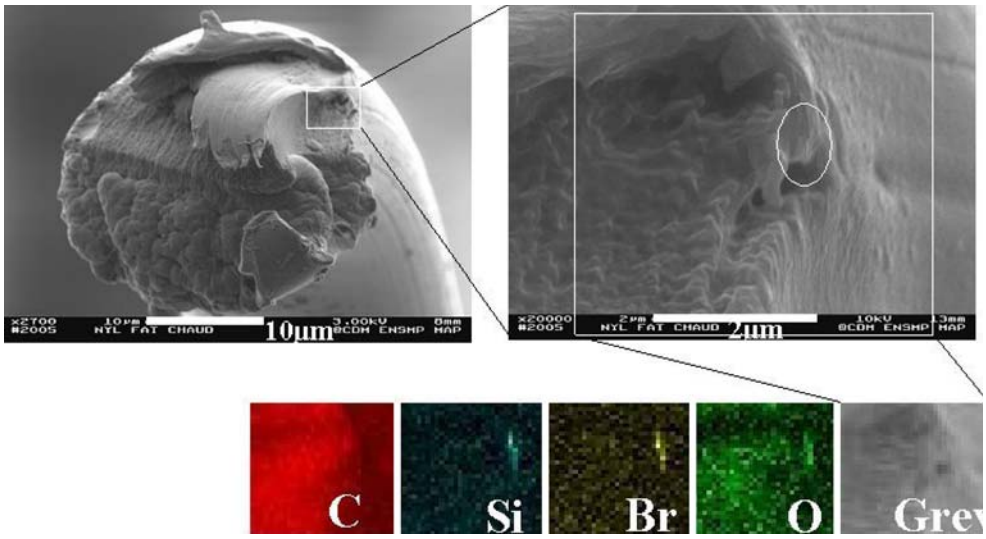

Fig. 11 SEM observation of fatigue failure morphology at 80 °C of PET fibres, with corresponding EDS X-ray map of C, Si, Br, O

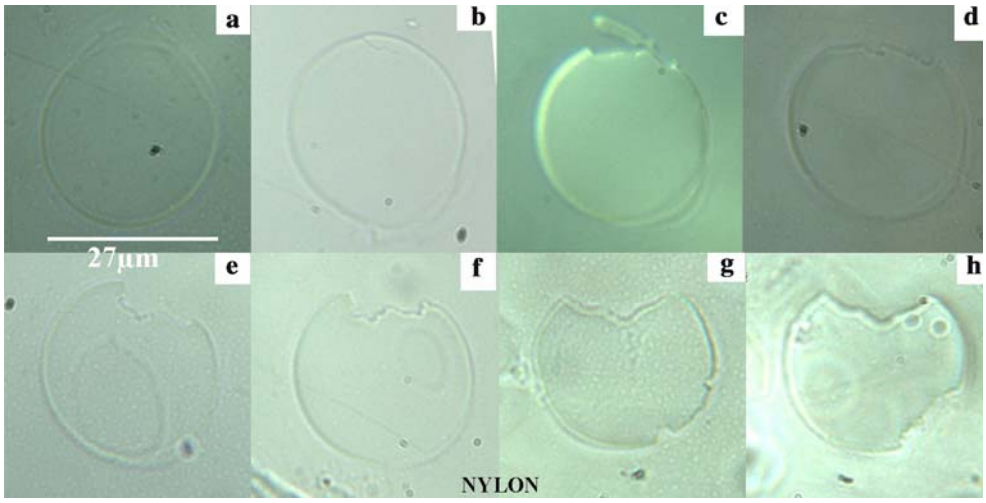

Fig. 12 Optical microscopy with natural light of sections of the complementary end of a fatigued nylon fibre. Section's thickness: 1.5 μm, in reverse order of the cut from the unaffected to failed part of the fiber

The complementary end of a PET_A fibre failed by fatigue was also sectioned with the microtome over a length of 250 μm. Four optical microscope images are shown in Fig. 13. The first was taken under polarized light. The fibre seems to show slight birefringence. However, a skin can be observed, as the colour of the side of the fibre section is different from that of the core. The birefringence reveals that the skin is locally damaged, as the colour is much clearer on the top of the section. In the other images, the crack penetrates increasingly inside fibre. A second crack can be seen to have initiated in the last image.

Discussion

All the as-received fibres contained inclusions of different sizes and natures. The number of inclusions in PA66 and PET_A was found to be fifty times fewer than in PET_B. It could be speculated that the large number of particles in this latter fibre indicates that they were there in the role of a filler or alternatively as a reinforcement. The sizes of the particles, as measured with optical or scanning electron microscopy, were between 0.4 μm and 1 μm, which are a significant fraction of the fibre diameters. In polyester fibres, antimony, in particle form, is used as a catalyst, and sub-micron TiO_2 particles may be included to modify the strain-induced crystallisation of the highly stretched polymer, as presented in the study of Taniguchi [8]. In PA66 fibres, silica particles were found sometimes associated with bromine; this element is known for its role as a flame retardant and antioxidant in polymers. Some other elements were detected, such as copper, zinc, sodium, phosphorus, but the exact sizes and shapes of the particles containing them could not be observed by optical microscopy, as they were less than 0.4 μm.

The important role played by these inclusions in fatigue crack initiation has been clearly demonstrated. Optical microscopy has revealed the presence of inclusions on the complementary ends of fatigued fibres near the initiation point, just under the surface (less than 2 μm from the surface). This was confirmed by an independent method using SEM observation and EDS analysis. The presence of inclusions is likely to create high shear stresses in the polymer matrix and locally weaken the structure. It is likely that repeated shear stresses in this highly anisotropic material

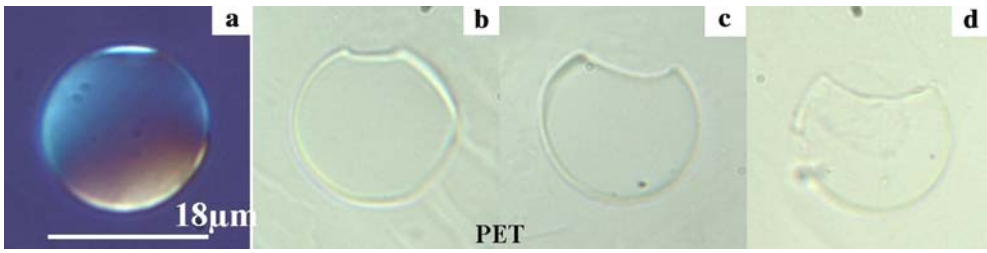

Fig. 13 Optical microscopy of sections of the complementary end of a fatigued PET fibre. Thickness of section: 1.5 μm, in reverse order of the cut the first one (**a**) is observed under polarisation to reveal a change of birefringence, the three others (**b–d**) are observed with natural light

initiates longitudinal cracking. The observations carried out by Herrera and et al. [2] on occasional fatigue fracture morphologies showing conical cracks initiated by a particle inside the fibres were the first revelation of the presence of particles near initiation points. The present work is a confirmation and a generalisation of the presence of solid inclusions necessary for crack initiation.

Fibre sectioning reveals the presence of a skin in PET_A and PA66 fibres. Polarized light allows a clearer view of this part of the fibre as is shown in Fig. 14. Under polarized light there is always a clear line which separates the skin from the core that is not observed under natural light. This separation appears at around 1 μm from the fibre surface. This is a proof of a strong change of birefringence between these two zones. The skin is always clearer than the core, which is a sign of greater birefringence. This skin must have different microstructural properties from those of the core and show a greater orientation. Observations, in polarised light, of complementary ends of failed fibres, after fatigue tests, have revealed a great variation of colours between the undamaged zone and the zone from where the tongue was removed, as shown in Fig. 15. This skin probably appeared during the crystallization of the molten polymer during spinning. This skin seems to result from the plastic deformation of the just crystallized polymer under elongation of the skin layer whilst the core crystallizes subsequently, under or just after flow. The higher orientation induced by plastic deformation seems to be the origin of this skin and of the discontinuity of birefringence along the radius.

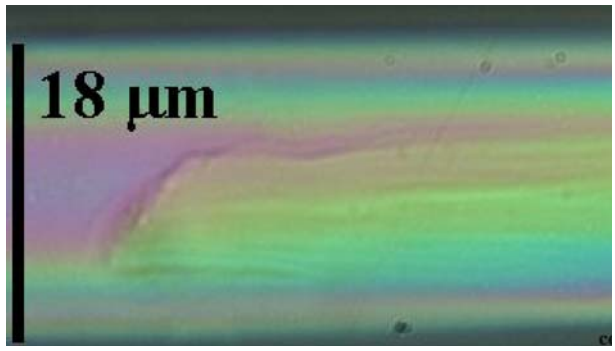

Fig. 15 Optical observation along the fibre axis of complementary end of PET fibre after failure under fatigue conditions, seen in polarized light

The fatigue crack initiation points at room temperature are localized at the interface between core and skin. The first stage of fatigue damage is the debonding of the skin; the first step of which is presented in Fig. 16 for PA66 (a, b, c) and PET_A (d, e). In PA66 fibres, the debonded region reveals that the skin is circumferentially compressed and that the interface between skin and core is weak. Shear stresses in this interfacial zone must be particularly damaging and the debonding probably releases internal stress. For PET_A fibres, the damage is also localised at the interface between the core and the skin for the first step however no debonded region has been observed for these fibres.

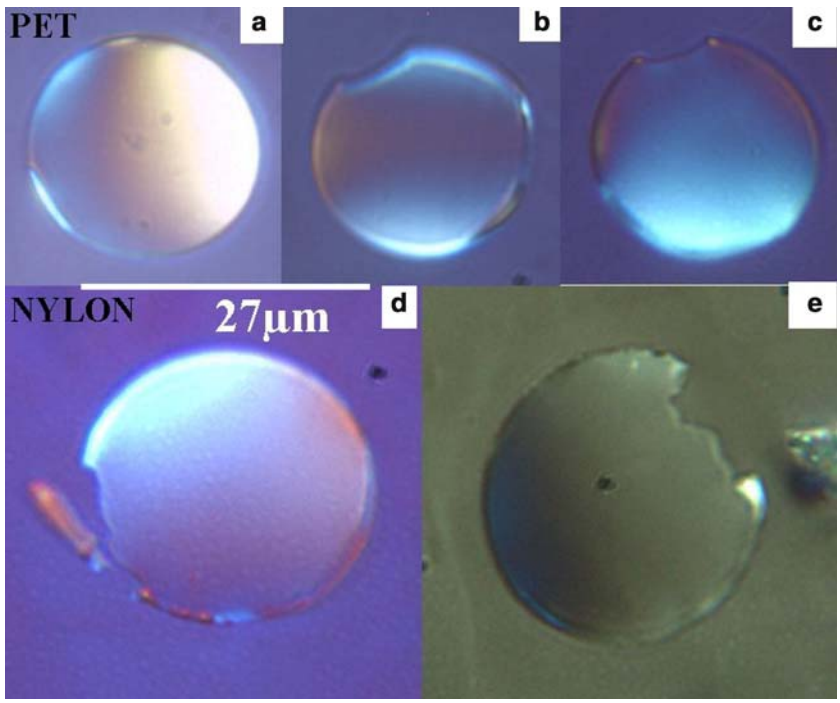

Fig. 14 Image of the skin/core structures by optical microscopy observations of microtomed sections of PET and PA66 fibres under polarized light

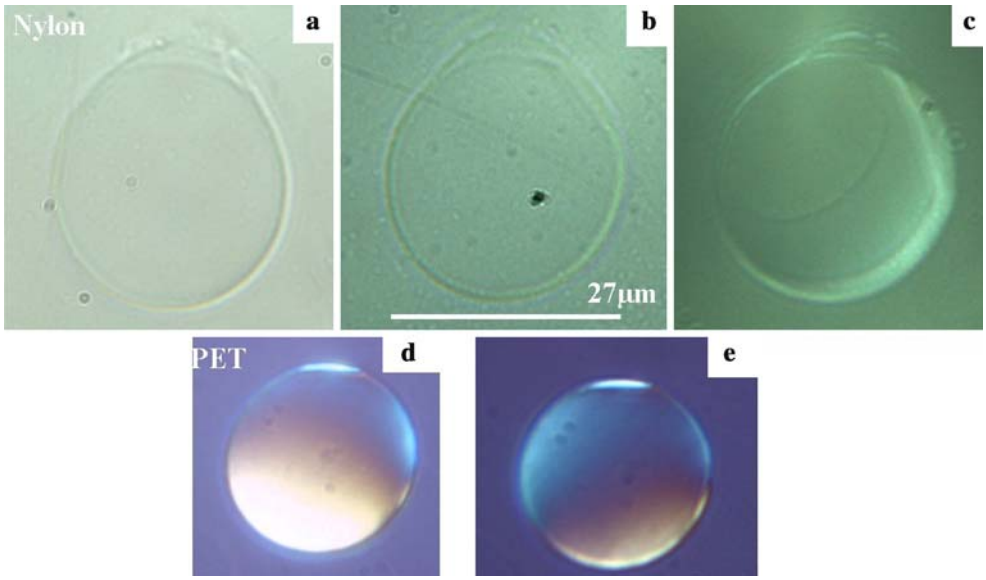

Fig. 16 First stage of damage in nylon or PET fibres subjected to fatigue, optical microscopy of microtomed sections of fibres (last three images under polarized light)

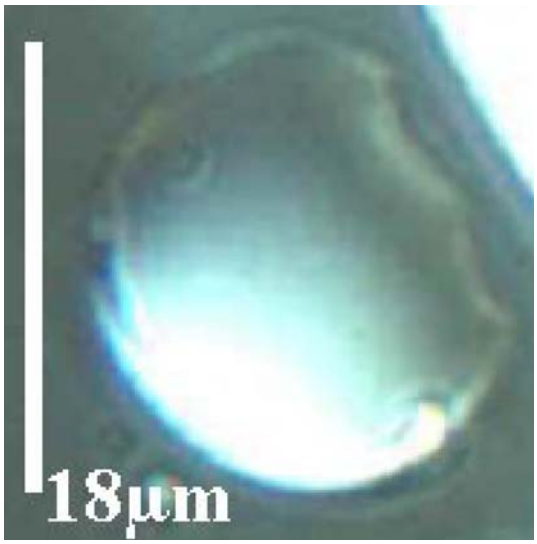

Fig. 17 Microtomed section of a PET fibre after fatigue failure, showing an inclusion associated with the crack

Figure 17 shows another example of a microtomed section of a complementary end of a PET fibre failed in fatigue; the tongue has been removed from the top right side of the image. Another crack, which does not emerge at the surface, can be observed on left side of the image and a particle can be observed just in the middle of the crack. This is further evidence that it is the combined effects of a weak interface between skin and core and an inclusion increasing shear stress that produces fatigue crack initiation.

The propagation process seems to have two different components at room temperature. The penetration of the crack can be discontinuous with steps inside the fibre due to the presence of particle near to the path of the crack. Such an instance is shown in Fig. 18. The images b and c in Fig. 18 show a section with a particle taken with various depths of focus, whereas images a and d are respectively upstream and downstream sections. In this case, an inclusion was close to the path of the longitudinal crack, and it modified the crack penetration. The penetration of the crack inside the fibre can also be continuous as in PET specimens' observations (cf. Fig. 13). Shear stress in isotropic material produces cracks angled at 45° however; in these highly anisotropic materials, the angle is seen to be much smaller.

The fatigue crack propagates under the effects of local inhomogenities and stresses and tends to form a

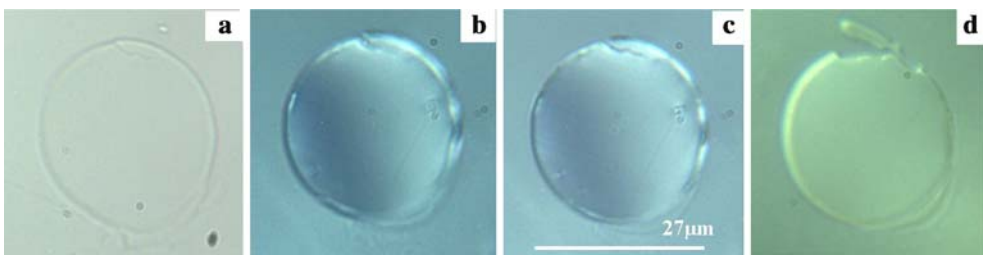

Fig. 18 Optical microscopy using polarised light of PA66 fibre sections from an unaffected zone (**a**) to a zone of fracture (**d**) revealing the role played by inclusions in crack propagation

smooth concave fracture surface, in the PET fibre. In case of irregularities in the concave shape of the longitudinal crack, the shear stress concentration created makes these defects disappear. An example is presented in Fig. 19; the irregular morphology observed in image a, due to discontinuous penetration, tends to disappear as shown in image f. Polarized light gives relevant details on this process as the colour is directly linked to the birefringence i.e. the local orientation. This residual orientation must be a sign of the plastic deformation undergone locally by the polymer during the propagation of the fracture. From image b to image e, the brightness and the localization of this plastic deformation increases. The more regular the crack shape, the less energy is needed for propagation.

Each solid inclusion does not necessarily lead to a crack during fatigue. One to four cracks are generally observed along a fatigued fibre of 30 mm length. Three explanations can be proposed for there not being more cracks. Firstly, it is probable that all the particles do not play the same role; there is discrimination in position but maybe also in nature. In Fig. 20, each microscopic observation is taken under polarized light in extinction conditions. The image on the left is of an as-received PET_B fibre showing tens of particles, but amongst them all only four are surrounded by a

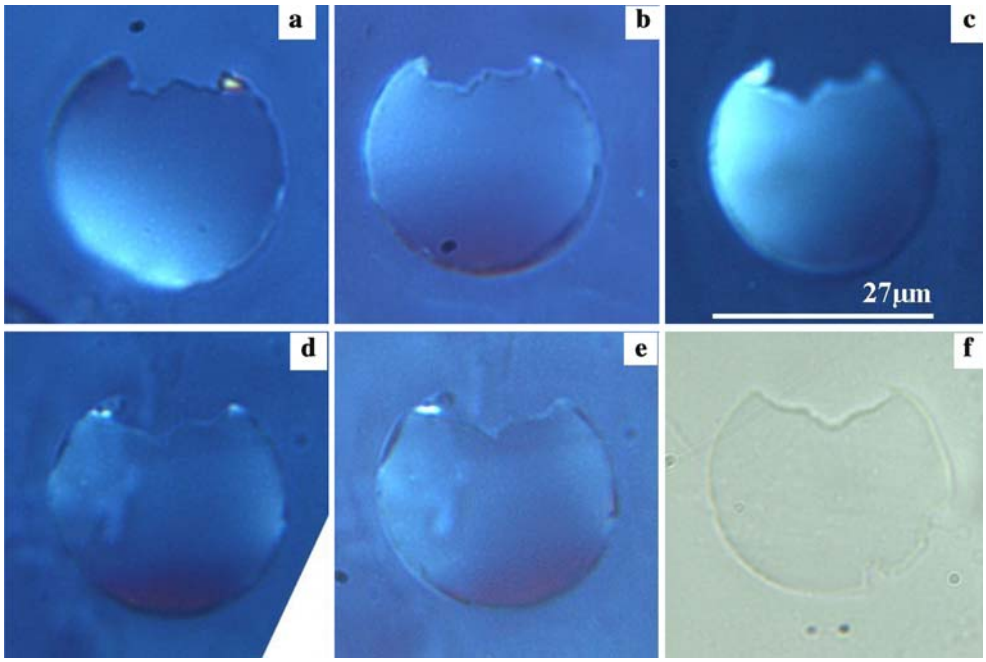

Fig. 19 Image of local variations of birefringence in a PA66 fibre section under polarized light

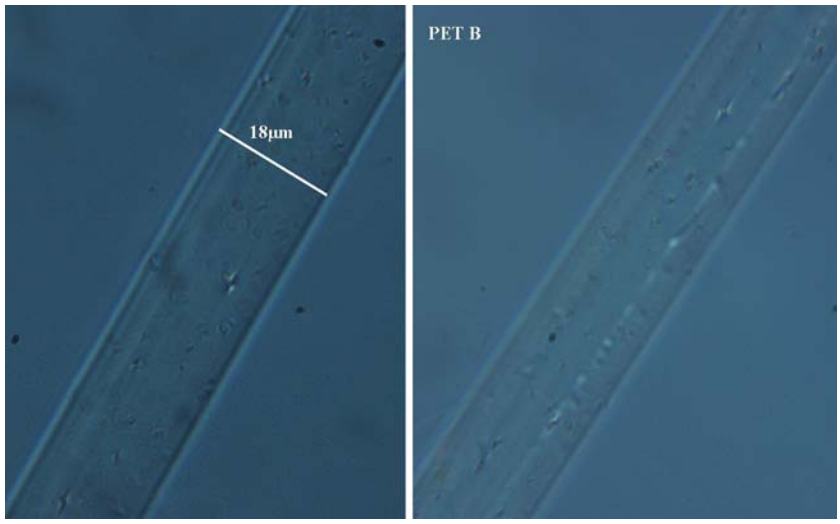

Fig. 20 Optical microscopy of PET_B fibres under polarized light, in extinction conditions. First image showing the as-received fibre and the second, the complementary end of fibre failed by fatigue

coloured zone in the shape of an eye corresponding to a modification of the surrounding polymer, which is probably less oriented or of lower density. The image on the right shows a complementary end of a PET_B fibre after fatigue failure and shows a particle with an eye shape just in the middle of the propagating crack. This inclusion participated in the crack propagation whereas the others did not. To provoke damage the particle must be at 1 μm or less from the skin. The nature of the interface between inclusion and matrix can also be of fundamental importance. Secondly, it is possible that there are numerous cracks all over the fibre subjected to the fatigue conditions inducing decohesion between the skin and the core but only a few emerge at the surface. Thirdly, as the first longitudinal crack emerges at the surface of the fibre, the translation symmetry is broken and the speed of propagation must increase preferentially compared to that of other cracks.

Conclusions

This study, based on mechanical fatigue tests performed on single fibres extracted from two polyester yarns and one polyamide yarn, has revealed more about the microstrucural processes involved in crack initiation. Numerous analyses were carried out on SEM images with EDS X-ray mapping and on images obtained by transmission optical microscopy on microtomed sections. This study has revealed the existence of a skin/core structure; the skin being about 1 μm thick or less, and made up of more oriented polymer than the core. It has been seen to be in circumferential compression as after debonding, it increases in length. This work has also revealed the presence of solid inclusions inside the fibres, which are the residues of catalysts or other active chemical or mechanical additives added during the production process. These particles were found to play a principal role in fatigue crack initiation. The fatigue crack could be associated with one or more particles both at initiation and during propagation. The interface between skin and core is seen to be weak so that repeated shear stresses in this region, if it contains a particle, are able to create damage by debonding between the skin and core which then develops into a longitudinal crack. This crack emerges at the surface and penetrates with a small angle into the fibre, so reducing the load bearing section until failure occurs by creep or tensile processes. This study generalises the role played by solid inclusions, observed by Herrera and al. [2] on a few cases, to the initiation of all fatigue cracks in both PET and PA66 thermoplastic fibres. Initiation and propagation of fatigue crack at hot temperature (80 °C and 120 °C) shortly evocated in this study will be developed in a paper to come.

Acknowledgement The authors wish to thank F. Grillon for his support for SEM observation.

References

1. Bunsell AR, Hearle JWS (1974) J Appl Polym Sci 18:267
2. Herrera Ramirez J, Bunsell AR (2005) J Mater Sci Lett 40:1269
3. Lechat C, Bunsell AR (2006) J Mater Sci 41(6):1745
4. Oudet C, Bunsell AR, Hagege R, Sotton M (1984) J Appl Polym Sci 29:4363
5. Le Clerc C, Piant A, Bunsell AR, J Mater Sci DOI 10.1007/s10853-006-0835-8
6. Duh B (2002) Polymer 43:3147
7. De Schryver D, Landry SD, Reed JS (1999) Polym Degrad Stab 64:471
8. Taniguchi A, Cakmak M (2004) Polymer 45:6647